Water Air Soil Pollut (2024) 235:450
https://doi.org/10.1007/s11270-024-07249-4

Manganese Ethylenediamine Phosphates Enhanced the Adsorption Capacity and Selectivity of Biological Soil Crusts for Cadmium

Ke Song · Bin Liu · Xiaolin Kuang · Huijuan Song · Qingru Zeng · Liang Peng

Received: 19 August 2023 / Accepted: 4 June 2024 / Published online: 20 June 2024

Abstract Biological soil crusts (BSCs) widely exists in mudflat environment, which is known to be efficient in capturing heavy metals from aqueous solutions; However, their ability to adsorb cadmium (Cd(II)) is limited due to low capacity and selectivity. To address this limitation, manganese ethylenediamine phosphates (MEPs) nanomaterial were incorporated into the BSCs to enhance Cd(II) uptake. The MEPs nanomaterials attached to BSC significantly improved the adsorption capacity, rate, and selection for Cd(II). The adsorption kinetics of Cd(II) by BSCs and BSCs-MEPs was well described by a pseudo-second-order model, with BSCs-MEPs exhibiting a much higher adsorption capacity for Cd(II) (77.00 mg/g) compared to BSCs (55.44 mg/g). The Cd(II) removal by BSCs-MEPs has been accelerated to 2 stages, in which the film diffusion/intraparticle diffusion/chemical reaction participated in the 1st stage. And another stage was dynamic equilibrium process. The adsorption isotherm of BSCs-MEPs demonstrated superior performance for Cd(II) compared to BSCs across a pH range from 2 to 9. Most importantly, even in the presence of high concentration of Na^+ or Ca^{2+} ions, BSCs-MEPs exhibited preferential adsorption for Cd(II), a result not observed with BSCs alone. Analysis of X-ray photoelectron spectroscopy spectra demonstrated that functional groups (-NH_2/-COOH/-OH) played an important role in Cd(II) adsorption, while the MEPs attach to BSCs leading to the -NH_3^+ deprotonation, thus enhanced the BSCs' affinity toward Cd(II). Furthermore, molecular dynamics simulation clearly showed that diffusion coefficients (D) of Cd(II) were much higher than those of Ca^{2+} in EPS with abundant -NH_2, which were responsible for selective adsorption. These findings might provide a valuable approach for treating Cd-contaminated water bodies.

Keywords Biological soil crusts · Nanomaterial · Cd(II) · Adsorption

1 Introduction

In recent decades, cadmium (Cd) contamination in soil and water environments has attracted worldwide attention since it can exert teratogenic and carcinogenic health risks to both humans and wildlife via bioaccumulation (Li et al., 2023; Mansoorianfar et al., 2022). Cd contamination in soil and water primarily stems from the discharge of low-treatment effluents from various industries, including mining,

Supplementary Information The online version contains supplementary material available at https://doi.org/10.1007/s11270-024-07249-4.

Ke. Song · B. Liu · X. Kuang · H. Song · Q. Zeng · L. Peng (✉)
Department of Environmental Science & Engineering, Hunan Agricultural University, Changsha 410128, P. R. China
e-mail: pengliang2004@126.com

waste incineration, industrial fertilizer production, and coal and oil combustion (Nabipour et al., 2023; Peng et al., 2021; Shirkhorshidi et al., 2023a). Especially, the Cd content in industrial wastewater, even in natural water, can be extremely high due to the excellent migration ability, solubility, and persistence (Kruglikov et al., 2019; Kumar et al., 2019; Tang et al., 2022; Teng et al., 2020). Hence, there is an urgent need for effective methods to remove Cd^{2+} ions from contaminated water. To date, different mechanism-dependent methods to remove Cd include but are not limited to adsorption (Zhang et al., 2021), ion exchange (Zawierucha & Nowik-Zajac, 2019), flotation (Yenial & Bulut, 2017), chemical precipitation (Liu et al., 2021c), electrochemistry (Tran et al., 2021), and membrane separation (Szczepański et al., 2021). However, in terms of both efficiency and economics, adsorption stands out as a widely accepted, cost-effective, and efficacious approach for removing Cd(II) (Saleh et al., 2022). The effectiveness of Cd(II) adsorption largely hinges on the presence of surface active sites, which play a crucial role in governing Cd(II) transfer in environmental media; thus, chemical rich in N, O, and S are commonly utilized to stabilize Cd due to their high affinity and complexing ability toward Cd(II) (Nabipour et al., 2023). Consequently, developing, optimizing, and improving Cd(II) adsorption by these chemicals to control Cd(II) environmental risk is significant.

As a wide distribution of a compound of soil components and biocenosis on environments, biological soil crusts (BSCs) were considered excellent cadmium adsorbents since they were abundant in adsorption sites that originated from various chemicals and could complex heavy metal ions (Büdel & Colesie, 2014; Li et al., 2017; Yang et al., 2016). For instance, previous research by Yang et al. (2015a) demonstrated that when initial concentrations of copper and cadmium were 10 mg/L, within just two hours of exposure, copper content in BSCs varied from the range of 145.20 mg/kg to 342.42 mg/kg, while cadmium content ranged from 101.75 mg/kg and 236.29 mg/kg. The mechanism by which BSCs retain Cd(II) has been extensively documented, highlighting the significant correlation between heavy metal adsorption capacity and the content of extracellular polymeric substances (EPS) as well as the types of internal functional groups (Nouha et al., 2016; Qu et al., 2022; Yang et al., 2015b; Yue et al., 2015). Functional groups within EPS, such as -COOH, -OH, $-NH_2$, and -SH, have been identified as likely participants in heavy metal adsorption (Cui et al., 2021; Wang et al., 2019). However, these functional groups in EPs are likely to change the surface charge to more positively by protonation originating from the decreasing pH values that could significantly affect the binding and adsorption ability of BSCs to heavy metals (Gan et al., 2015; Kuang et al. 2020). These studies provide foundational theory for understanding variations in the Cd(II) adsorption capacity by BSCs under different pH conditions. However, few studies have addressed how to enhance the removal rate of Cd(II) against the change of pH that, commonly considered the availability of functional groups for heavy metal adsorption only altered with pH. Further research is still required to examine the changing availability of functional groups for Cd(II) adsorption reactions by posing an impact on these active sites other than pH.

Due to the unique physical and chemical characteristics of nanomaterials, which have extensive properties of nanoparticles such as high porosity, reactivity, and surface area etc., nanotechnology has introduced a new treatment strategy for Cd(II) contamination (Kumar et al., 2021). Apart from their adsorption capabilities, nanomaterials have been widely reported has a facilitating effect on removing cadmium by improving the growth of biology or increasing biological resistance to cadmium, which are inextricably related to EPs (Gao et al., 2013). Song et al. (2022) have clearly demonstrated that the adsorption capacity of Cd(II) by BSCs is largely enhanced by TiO_2 nanoparticles occurring in a simple system; they also believed that extracellular substances play a crucial role in the adsorption of Cd(II) without further discussion in the origination of that enhancement. Indeed, these positive charge nanoparticles tend to interact easily with the negative charge of EPs substances, which mainly originated from functional groups such as $-NH_2$/-COOH/-OH found in polysaccharides or proteins (Fulaz et al., 2019). Nonetheless, it was unknown whether this interaction from NPs could generate what impacts direct at those functional groups and how it will subsequently influence the adsorption of Cd(II). Besides, the natural environment is complex, with various inorganic ions and cadmium ions coexisting, which have been shown to significantly reduce Cd adsorption by competing for adsorption sites (Imran et al., 2020).

From the considerations above, this study aims to investigate a strategy to enhance the selectivity and capacity performance of BSCs for Cd(II) adsorption, given their widespread presence in the environment. Manganese ethylenediamine phosphates (MEPs) are chosen for the modification of BSCs due to their large surface area, cost-effective availability, and low toxicit. The Cd(II) adsorption capacity and selective of BSCs-MEPs matrix are evaluated through adsorption kinetics, isothermal and pH/ions sensitivity experiment. Moreover, X-ray photoelectron spectroscopy has been employed to analyze variations in functional groups on BSCs-MEPs, and the selective adsorption of Cd is demystified through molecular dynamics simulation.

2 Materials and Methods

2.1 Reagents and Materials

The BSCs used in this study were collected from paddy fields in Huang-Gu (HG; N27°34′28", E113°12′58") in Hunan Province, China. All experiments utilized analytical reagent-grade chemicals commercially available. MEPs was synthesized by following processes, briefly, the ethylene glycol (EG) mixed solution of 20 mL was first dispensed by dosing known amounts of ethylenediamine ($C_2H_8N_2$) and phosphoric (H_3PO_4), which contained 0.03 and 0.011 mol of $C_2H_8N_2$ and H_3PO_4, respectively. Subsequently, a 0.25 M $MnSO_4$ (40 mL) was dropwise added to the EG mixed solution (at a rate of 1 mL min^{-1}) under sustained vigorous stirring. The reaction proceeded at 80 °C for 10 h and, MEPs was collected from white precipitate, followed by repeated washing with ultrapure water and absolute ethanol. The obtained MEPs was finally dried at 60 °C for 12 h. The BSCs-MEPs surface complex prepared for this study was of agglomerate gathered by mixed BSCs with MEPs, a mixture was formed by stirring BSCs with MEPs at 180 rpm for 1 h. The mixture consisted of 1.0 g of BSCs and 0.01 g of MEPs simultaneously mixed in a flask containing 100 mL of ultrapure water.

2.2 Batch Adsorption Experiments

The adsorption experiments were repeated three times under identical conditions, and the average data were plotted, with error bars representing the calculated standard deviation. Cd(II) adsorption isotherms were conducted in 150 mL glass beakers containing 1.00 g of BSCs and BSCs-MEPs, respectively, in a 100 mL Cd solution ($C_{Cd(II)}$ ranging from 5–200 mg L^{-1}). The pH of reaction was adjusted to 6.0 and maintained by dropwise addition of 0.01 M HCl and 0.01 M NaOH. After acting 36 h, the concentration of Cd(II) in the supernatant was determined by atomic absorption spectroscopy (AAS-990, CN) following centrifuging at 12,000 rpm for 10 min. The adsorption isotherm of Cd(II) was then analyzed with Langmuir (Eq. (1)) and Freundlich isotherm (Eq. (2)) model, and the formulae are as follows:

$$Q = \left(Q_e bC\right)/(1 + bc) \tag{1}$$

where Q and Q_e are the unit BSCs (and etc.) adsorption amounts of Cd(II) and, the maximum theoretical amount of Cd(II) that may be adsorbed, respectively, K is Langmuir constant, C deputes the equilibrium concentration of Cd(II).

$$Q = KC^{1/n} \tag{2}$$

where Q is the unit BSCs (and etc.) adsorption amounts of Cd(II), K is Freundlich constant, 1/n represents the adsorption intensity and, C is the concentration of Cd(II) at equilibrium time.

The adsorption kinetics of Cd(II) by BSCs and BSCs-MEPs, was initiated in a total volume of 100 mL of the reaction system at pH 6. The reaction system contained 100 mg/L Cd(II) and 0.1 g L^{-1} BSCs/BSCs-MEPs. At specified time intervals, 1.0 mL of suspension was extracted and subsequently filtrated with a nylon filter to analyze Cd(II) concentrations in the solution. The pseudo-second-order (PSO, Eq. (3)), pseudo-first-order (PFO, Eq. (4)), liquid film diffusion (LFD, Eq. (5)), intra-particle diffusion (IPD, Eq. (6)) and chemical reaction (CR, Eq. (7)) models were employed to further evaluate the interaction of Cd(II) with BSCs etc., with the equations as follows:

$$Q_t = \left(Q_e^2 kt\right)/\left(1 + kQ_e t\right) \tag{3}$$

$$Q_t = Q_e\left(1 - e^{-kt}\right) \tag{4}$$

where Q_e and Q_t are the amounts of adsorbed Cd(II) by BSCs (and etc.) at each reaction time and equilibrium time, respectively; k is the rate constant.

$$ln(1 - Q_t/Q_e) = -kt + A \quad (5)$$

where Q_e and Q_t are the amounts of adsorbed Cd(II) by BSCs (and etc.) at each reaction time and equilibrium time, respectively; k is diffusion rate constant; A is diffusion constant.

$$Q_t = kt^{0.5} + C \quad (6)$$

where Q_t refers to the amounts of adsorbed Cd(II) by BSCs (and etc.) at each reaction time; k is diffusion rate constant; C is a constant referring to characteristic of boundary layer.

$$1 - \left(1 - Q_t/Q_e\right)^{1/3} = kt \quad (7)$$

where Q_e and Q_t are the amounts of adsorbed Cd(II) by BSCs (and etc.) at each reaction time and equilibrium time, respectively; k is chemical reaction rate constant.

Based on the determined equilibrium time, the impact of pH and cation (Na^+ and Ca^{2+}, ranging from 0–100 mM) on the adsorption of Cd(II) (100 mg L^{-1}) by BSCs and BSCs-MEPs were assessed following the same procedures. Additionally, as a reference, the adsorption experiment of Cd(II) by 0.2 g L^{-1} MEPs was conducted under varying pH and cation conditions using the same experimental method.

2.3 Characterization Method

Constituent materials were characterized in each case using scanning electron microscopy (SEM; JSM-6380LV, Tokyo, Japan). Elemental species analysis was then conducted using an X-ray photoelectron spectrometer (XPS) (K-Alpha 1063, Thermo Fisher, UK). Sample preparation and measuring parameters followed the protocols outlined in previous studies (Liu et al., 2021b). Crystal forms of all materials were then determined using a Rigaku-TTRIII diffractometer (JPN), and the concentration of Cd in each solution under test was analyzed using atomic absorption spectrophotometer that configurated the flame atomiser (AAS-990, CN) and graphite furnace atomiser (GFAAS, PerkinElmer, USA).

2.4 Models and Simulation Methods

All theoretical calculations presented in this paper were conducted through molecular dynamics (MD) simulations using Accelrys software Materials Studio (version 6.0) (Chang et al., 2012). The single molecular structures of polysaccharides containing -COOH/-OH, -NH_2/-OH, and -PO_4/-OH are depicted in Fig. S1a-c, respectively, while the interactions of metal ions with water molecules to form $Ca^{2+}(H_2O)_4(OH^-)_2$ and $Cd^{2+}(H_2O)_4(OH^-)_2$ complexes (Song et al., 2012) are illustrated in Figs. S2, respectively. These single polysaccharide molecules were constructed using an EPS film model and amorphous cell calculation with a density of 1.0 g/cc. This model incorporated a total of ten polysaccharides as well as two $Ca^{2+}(H_2O)_4(OH^-)_2$ and $Cd^{2+}(H_2O)_4(OH^-)_2$ complexes, respectively. The condensed-phase optimized molecular potential for atomistic simulation studies (COMPASS) force field was employed to conduct energy minimizations and MD calculations, with the NVE ensemble used throughout. Each calculation had a time step of 1.0 fs, and was performed for 5.0 ps; the mean-squared displacement (MSD) of Ca(II) and Cd(II) in the EPS model can be analyzed using the Einstein relationship, as follows:

$$D = \frac{1}{6}\lim_{r\to\infty}\frac{d}{dt}[(r_i(t + t_0) - r_i(t_0)]^2 \quad (8)$$

In this expression, N denotes the total number of atoms, while $r_i(t_0+t)$ and $r_i(t_0)$ refer to positions at time t_0+t and time t_0, respectively. Similarly, B is a constant, and D denotes the self-diffusion coefficient.

3 Results and Discussion

3.1 Characterization of BSCs, MEPs, and BSCs-MEPs

The morphologies characteristic of BSCs, MEPs, and BSCs-MEPs revealed by SEM are shown in Fig. 1. In the collecting BSCs, filamentous structures and a significant fibrous texture are evident. These features are likely attributed to a combination of microorganisms such as cyanobacteria, microalgae, cryptogams, and extracellular polymeric substances, possibly integrated with minerals or other

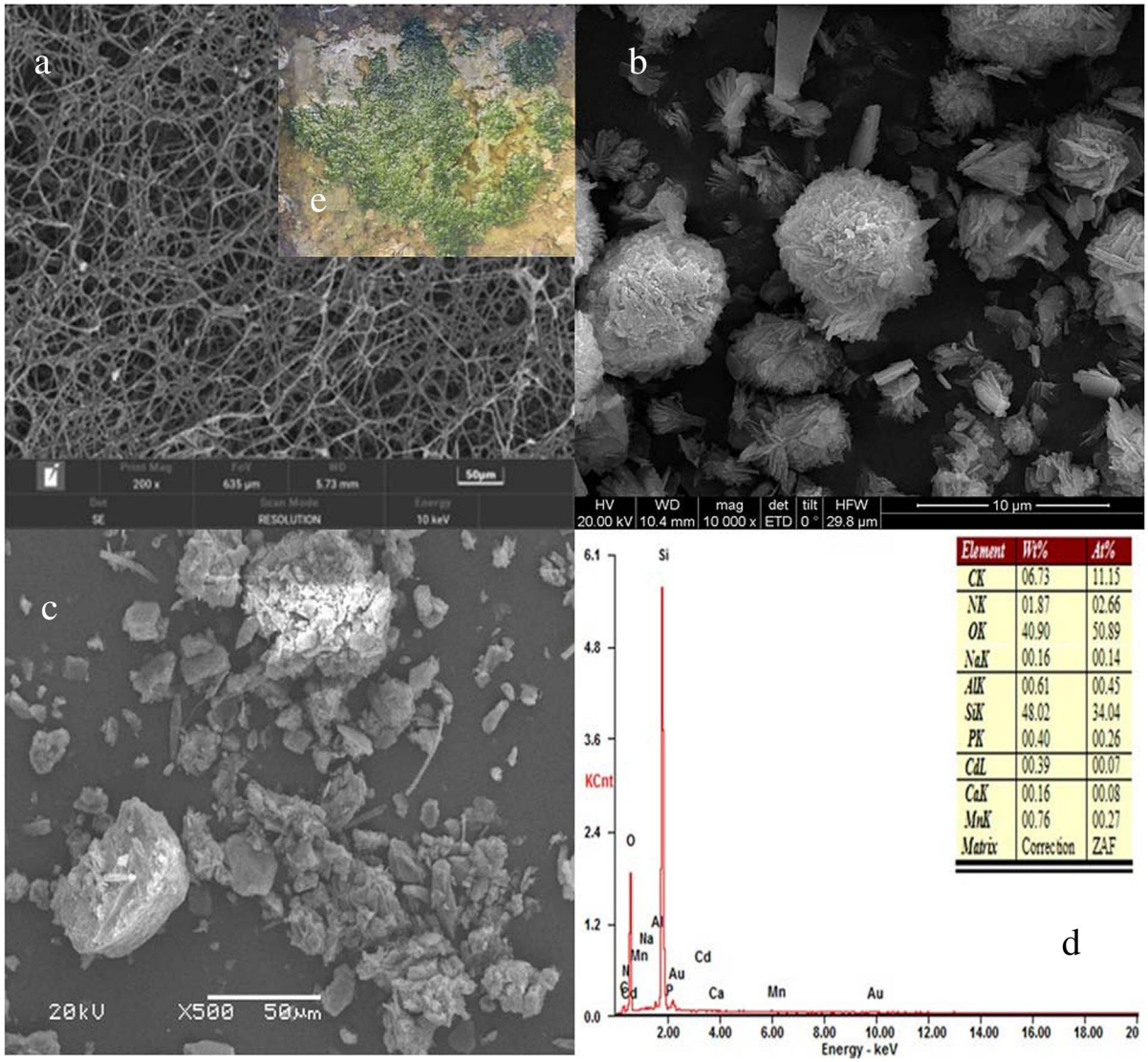

Fig. 1 The SEM images of BSCs (**a**), MEPs (**b**), BSCs-MEPs (**c**) and, the EDS analysis of BSCs-MEPs (**d**), where the insertion diagram (**e**) was the BSCs photo gathered from its original environment

inorganic components (Warren et al., 2021). MEPs appear as aggregated particles with a diameter ranging from 5 to 7 µm, exhibiting a whitened appearance. The BSCs-MEPs composite shows the surface of BSCs covered with an additional layer of white material, indicating dispersion of MEPs onto the BSCs surface. Moreover, the amount of the dominant elements O, Si, C, N, and Mn were 50.89at%, 34.04at%, 11.15at%, 2.66at%, and 0.27at%, detected by EDS (Fig. 1d). The detection of Mn suggests the incorporation of MEPs within the BSC, as this element is not typically found in such crusts.

For reference, details in surface area and pore volumes of MEPs were summarized in Fig. S3 and Table S1, and this MEPs has a surface area of 262.62 m^2/g, a pore volume of 0.38 cm^3/g. The richness and diversity of bacteria have also been examined, as detailed in Fig. S4. Results indicate Cyanobacteria (41.14%) are the principal flora in BSCs while the unclassified bacteria of "f" Familyl is subdominant

bacterium and, few other genera are known (Rhizobiales, Leptolyngbya, Proteobacteria, ~ 1%-8%). These findings align with previous surveys indicating the prevalence of Cyanobacteria and Proteobacteria in BSCs (Tang et al., 2021; Tiwari et al., 2019).

3.2 Adsorption Kinetic and Isotherm of Cd(II)

At the onset of the reaction, Cd(II) was promptly adsorbed by BSCs etc., then slow adsorption until the end of the reaction was later (see Fig. 2a, detailed parameters listed in Table 1). Most of Cd(II) (39.10 mg/g) has been adsorbed by BSCs within 1 h, accounting for 70.53% of the equilibrium adsorption capacity (55.44 mg/g) observed after 24 h. For BSCs-MEPs, Cd(II) adsorbed not only shows likewise but also more rapidly, which the adsorption capacity obtained at the reaction of 1 h (76.40 mg/g) accounting for 99.22% of the equilibrium amount (77.00 mg/g). The adsorption rate of Cd(II) by BSCs-MEPs, obviously higher than that by pure BSCs, was apparent. It was observed that kinetic models provided a better description of Cd(II) adsorption on BSCs-MEPs compared to pure BSCs, indicating a more complex adsorption process in the BSCs system. Previous studies have suggested that Cd(II) adsorption could be further divided into three stages resulting from the synergetic control of liquid film diffusion, intraparticle diffusion, and chemical reaction (Liu et al., 2021a). Considering these factors, Cd(II) adsorption kinetic were sequentially explored employing liquid film diffusion etc., as shown in Fig. S5 and Table S2. In the BSCs system, a typical 3-stage adsorption process emerged. With 1st and 2nd stages corresponding to intraparticle diffusion and film diffusion/intraparticle diffusion/chemical reaction, respectively. And 3rd stage was in a chemical equilibrium process. However, the adsorption of Cd by BSCs-MEPs has converted into two stages, comprising a rapid initial reaction followed by dynamic equilibrium (see Fig. S5). The adsorption of Cd(II) by BSCs-MEPs in the first stage was co-affected by the aforementioned procedures and, in this very stage, the amount of adsorbed was abruptly increased (76.40 mg/g) to reach the equilibrium stage within 1 h. It is, suggesting that MEPs significantly enhance the BSCs' affinity toward Cd(II) and, resulting in rapid adsorption.

Accelerated by MEPs, the BSCs exhibited a notably enhanced Cd(II) adsorption capacity compared to pure BSCs, as evidenced by the adsorption isotherm (Fig. 2b). The adsorption isotherm data were fitted to the Langmuir and Freundlich isotherm models. The relatively high correlation coefficient ($R^2 = 0.9825$)

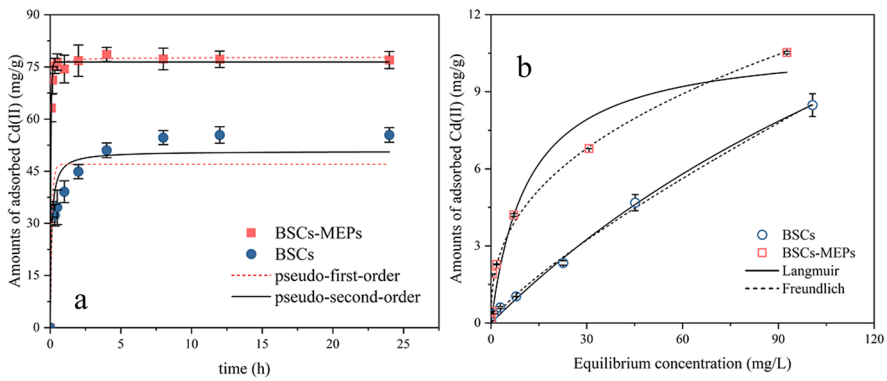

Fig. 2 Adsorption kinetics of Cd(II) (**a**) and isotherm (**b**) by BSCs and BSCs-MEPs

Table 1 Determined parameters and regression coefficients R^2, k and Q_e of pseudo-first-order model and pseudo-second-order model of BSCs and BSCs-MEPs

	Pseudo-first-order			Pseudo-second-order		
	Q_e (mg/g)	k_1 (min^{-1})	R^2	Q_e (mg/g)	k_2 (g mg^{-1} min^{-1})	R^2
BSCs-MEPs	76.4258	20.1860	0.9963	77.7548	0.7336	0.9978
BSC	46.9894	8.2980	0.7531	50.7557	0.1999	0.8708

for the BSCs-MEPs system indicated a strong fit with the Freundlich isotherm model (Table 2), implying that the adsorption of Cd(II) by BSCs-MEPs involves a broader range of mechanisms (e.g.: ion exchange, precipitation, complexation, and etc.) (Liu et al., 2021a). Nevertheless, both the Freundlich and Langmuir isotherm models effectively described Cd(II) adsorption onto BSCs. The correlation coefficients derived from the Langmuir isotherm model ($R^2 = 0.9968$) were comparable to those from the Freundlich isotherm model ($R^2 = 0.9973$). These findings align with the results of the kinetic study that, illustrate MEPs effectively alter the adsorption behavior of Cd(II) over BSCs. Moreover, the adsorption intensity (1/n) was determined to be 0.8023 (approaching 1) and 0.3916 over BSCs and BSCs-MEPs, respectively, indicating that the Cd(II) was more readily adsorbed by BSCs-MEPs compared to BSCs (Metwally & Rizk, 2014).

3.3 Cd(II) Removal Under Changing pH and Possible Cation Interference

3.3.1 pH Influence

The removal rate of the target metal warrants further study due to the changing pH value in natural environment. As shown in Fig. 3, the removal rate generally increased with pH within the tested range, it could be reasonably explained by the competition between Cd(II) and H^+ that compete for active surface sites of BSCs etc., in a lower pH solution (Elanchezhiyan et al., 2021; Karthik & Meenakshi, 2015). Conversely, in higher pH solution (>6), the binding sites tend to deprotonate, making them more accessible for the formation of inner/outer-sphere complex with metal ion and facilitating the formation of hydrolytic species of Cd(II) favoring its adsorption (Abate & Masini, 2005). Utilizing BSCs-MEPs is more advantageous for removing Cd(II) from the solution. The average Cd(II) removal rate in the pH range of 4–8 was 51.12% and 72.50% over BSCs and BSCs-MEPs, respectively. Even at relatively low pH values (2–4), the average Cd(II) removal by BSCs-MEPs is 1.29 times that by BSCs. Note that cadmium hydroxide could be produced when the solution pH exceeds 6, which could enhance cadmium removal to a certain extent (Hu et al., 2019). However, both MEPs and BSCs decreased the Cd(II) removal as pH was respectively exceeded 6 and 7, while BSCs-MEPs maintained a stable level even when the pH was increased to 9. This observation suggests that the overall effectiveness of cadmium removal by BSCs-MEPs is expected to be less influenced by increasing pH. Another observation is that cadmium adsorbed onto MEPs under lower pH (<4) is more variable than BSCs and BSCs-MEPs. Functional groups such as -COOH, -OH, $-NH_3$, and -SH are known active sites primarily involved in metal ion adsorption (e.g., Cd, Cu, Pb, etc.) (Gillan, 2016; Igiri et al., 2018; Shirkhorshidi et al., 2023b; Wyatt et al., 2014). These active sites with varying protonation abilities act as lewis base in forming inner/outer-sphere complex

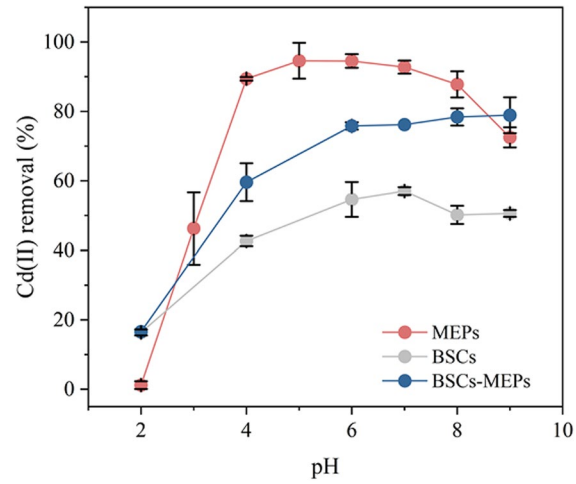

Fig. 3 Cd(II) removed by BSCs, MEPs, and BSCs-MEPs as a function of pH

Table 2 Langmuir and Freundlich isotherm model constants and correlation coefficients for adsorption Cd(II) in BSC and BSC-NMP

	Langmuir			Freundlich		
	Q_m (mg/g)	K (L/mg)	R^2	K_f [(mg g^{-1}) (mg $L^{-1})^{-n}$]	1/n	R^2
BSCs-MEPs	10.9794	0.0863	0.9312	1.7935	0.3916	0.9825
BSCs	26.7538	0.0046	0.9968	0.2105	0.8023	0.9973

with ion metal, which necessarily affects ion metal adsorption and therefore shows a mitigating effect on the adsorption of ion metal against the pH change (Martinez et al., 2002). This implies that Cd(II) removed by BSCs-MEPs (as well BSCs) is involved with more functional groups rather than just -NH_2 or any others.

In summary, the BSCs complexed with MEPs exhibit superior performance in the removal of Cd(II) across all pH levels, with the composite (BSCs-MEPs) demonstrating greater resistance to acidic conditions compared to raw BSCs.

3.3.2 Cation Influence

A significant concern regarding cadmium removal by whatever material is that, the cation co-presented with the heavy metal ions in natural waters is ubiquitous, which can vastly decrease the adsorption efficiency of cadmium ions (Imran et al., 2020). In addressing this issue, both $Ca(NO_3)_2$ and $NaNO_3$ were used as representative strong electrolytic salt to investigate effect of coexisting cations on Cd(II) adsorption over BSCs-MEPs, etc. Surprisingly, the enhanced salinity resistance of BSCs-MEPs appears to be unaffected by the presence of Na^+ or Ca^{2+} ions, potentially due to their selective adsorption capacity for Cd(II) compared to MEPs and BSCs alone. As depicted in Fig. 4, the Cd(II) removal efficiency decreased from 89.49% to 74.82% in the system with 25.0 M $Ca(NO_3)_2$ and BSCs-MEPs, remaining nearly constant (~70%) as the Ca^{2+} concentration gradually increased to 100.0 M. Conversely, the increasing Na^+ concentration seems not to affect the Cd(II) removal (~88%) by BSCs-MEPs. However, following the addition of 25.0 M Ca^{2+}, the efficiency of MEPs and BSCs for Cd(II) removal sharply decreased to very low values of 16.50% and 15.67%, respectively, with the removal efficiency was determined to 12.30% and 14.95% after 100.0 M Ca^{2+} addition. Moreover, Na^+ addition resulted in a decrease in Cd(II) retention by BSCs and MEPs of 6.26%-18.31% and ~ 19.49%, respectively. Lu et al. (2012) suggest that the monovalent interfering ions (e.g.: K^+, Na^+) are likely form outer-sphere complexes. Because of their lower charge, these monovalent ions also had a relatively weak electrostatic attraction toward the adsorbent surface. So, these net results of monovalent ions weakened their affinity with the adsorbent surface, Na^+ therefore slightly affected the adsorption of Cd(II) over BSCs-MEPs etc. Previous studies have also shown that the presence of Na^+ mainly decreased adsorptive Cd(II) via an ion exchange interaction (Wu et al., 2023), this result implies that Cd(II) adsorption onto the BSCs-MEPs mainly occurs via complexing interaction rather than ion-exchange. However, the chemical-physical characteristics of Ca^{2+}, such as its ionic radius and hydrodynamic radius, are similar to those of Cd(II), which leads to close even higher removal rate of Ca^{2+} from paddy fields, compared to Cd(II) (Peng et al., 2020). To our knowledge, this is the first instance where a combination of MEPs with BSCs has demonstrated favorable Cd(II) adsorption in the presence of Ca^{2+} interference.

3.4 Adsorption Mechanisms Study

It must be a collaborative effort for the adsorption of Cd(II), as evidenced by the high-efficiency removal achieved by the combination of MEPs and BSCs (Fig. 2). Based on this premise, cadmium should be evenly adsorbed onto the BSCs-MEPs

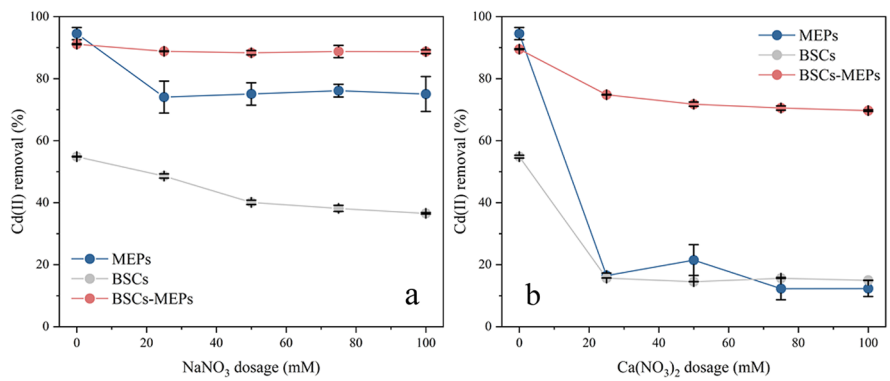

Fig. 4 Effect of Na^+ (**a**) and Ca^{2+} (**b**) on Cd(II) removal by BSCs, MEPs, and BSCs-MEPs

matrix while being distinctly concentrated at MEPs' location. We observed the distribution of elements (P and Cd, in which P mainly derive from MEPs.) in the BSCs-MEPs sample following Cd(II) adsorption within a micro-area, confirming that cadmium was widely distributed in the material matrix surface (Fig. 5). Furthermore, as Mn was used as a proxy for the distribution of MEPs, an element absent in pristine BSCs, it was clear that cadmium was closely associated with MEPs. Though that connection between Cd and MEPs appears strong, we propose that not all of the Cd(II) in the solution was adsorbed by MEPs due to the universally dispersed C or N element as well as Cd. A plausible interpretation is that Cd should not be sufficient to displace Mn from MEPs due to the solubility of the reaction product. Metal ions interact with polyvalent metal ions via an ion-exchange mechanism that only occurs when a higher hydrolytic stability species is produced. (Shashkova et al., 1999). Therefore, the high response intensity of Al seems irrelevant to Cd, while the lower response intensity of K and Mg is negligible in influencing Cd adsorption. Cd(II) is thus more possibly to interact with other ligands present in EPs (e.g., -NH_2, -COOH, -OH) (Yan et al., 2022), and MEPs influent adsorption indirectly by changing the adsorption behavior.

As discussed above, element information was explored by analysing X-ray photoelectron spectroscopy spectra (XPS) to verify the adsorption behavior of Cd(II) over BSCs-MEPs. The XPS survey spectrum of BSCs, BSCs-MEPs, and BSCs-MEPs-Cd(II) spectra were carried out as shown in Fig. S6, which generally exhibited responses from C 1 s, O 1 s, N 1 s, P 2p, and Mn 2p extranuclear electrons, with the peak of Mn 2p only observed in BSCs-MEPs sample. Phosphorous, known to exist in biomass in quantity, was detected in the BSCs sample by XPS, while its high-resolution spectra showed no difference between these samples and, more details will be discussed later (Vassilev et al., 2023). The Cd 3p and 3d peaks seen in BSCs-MEPs-Cd(II) matrix only and its spectra of high-resolution for 3d electron orbit is shown in Fig. S7, which confirms the adsorbed of Cd(II) by BSCs-MEPs.

The case of binding with Cd(II) through the coordination of functional groups has been definitively established in prior works (Mathivanan et al., 2021). This interaction between Cd and function group also plays a fundamental role in the adsorption of BSCs-MEPs, as revealed by the differences observed in pre- and post-adsorption scan spectra (Fig. 6). The C 1 s deconvolution of pre-adsorption BSCs showed peaks at 284.8 eV,

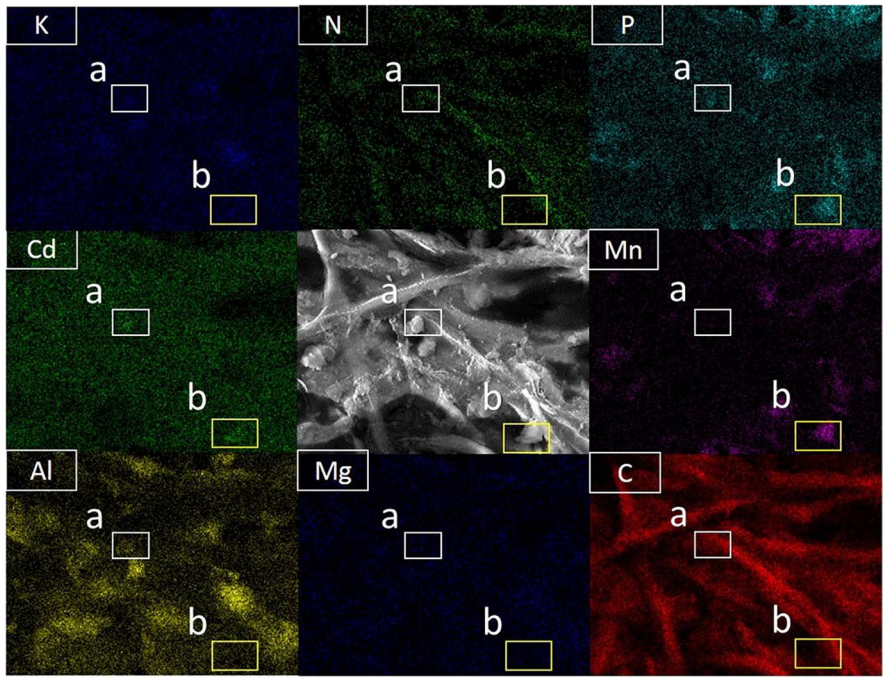

Fig. 5 SEM-Mapping plots of BSCs-MEPs after adsorption, in which the small box are some areas of Cd concentrate in

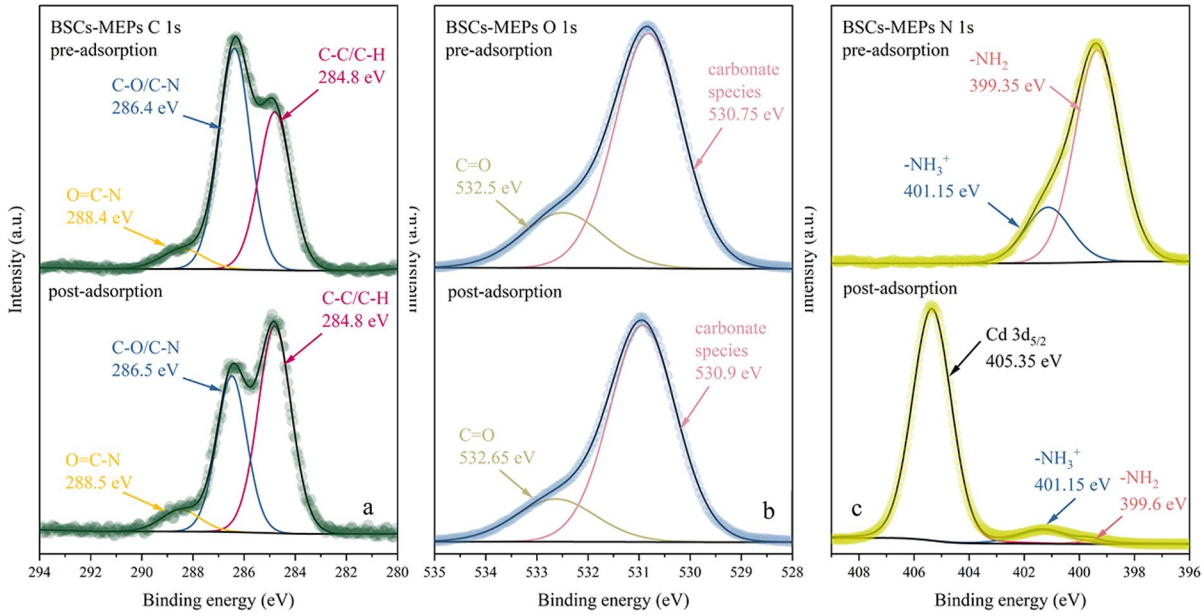

Fig. 6 High-resolution XPS spectrum of C (**a**), O (**b**), N (**c**) pre- and post-adsorption of Cd by BSCs-MEPs

286.4 eV, and 288.4 eV, attributed to the C–C/C-H, C-O/C-N, and O = C-N species, respectively (Lian et al., 2022). After adsorption, the main changes observed in the C 1 s spectra were the shift of the peak at 286.4 eV (-C-N) to 286.5 eV and the peak at 288.4 eV (O = C-N) to 288.5 eV. This indicates the involvement of C-N and O = C-N functional groups in the adsorption of Cd(II) by BSCs-MEPs. In addition to the shift of binding energy, an apparent decrease in the ratio of bands of C-O/C-N has been observed, suggesting the possibility formed of Cd–O or a weak interaction between -NH_2-Cd species and -OH (Das et al., 2007; Guo et al., 2017). Figure 6b shows the O 1 s spectrum de-convoluted to be two peaks at 530.75 eV and 532.5 eV representing metal carbonate species and C = O bonds (Rao et al., 2012; Yan et al., 2018), respectively, which shifted to 530.75 eV and 532.65 eV after adsorption of Cd, respectively. The change in the metal carbonate peak is presumes to be due to the formation of cadmium carbonate species, which may be negligible to the adsorption of Cd(II) since the slight change in the peak, while the shift of C = O further confirms its participation in the sorption process by bonding to Cd(II). Binding energy move to a higher one was also observed for -NH_2 (399.35 eV to 399.6 eV) after adsorption (Fig. 6c). The lone pair of electrons in the ligands (O and N atom) was donated to the empty electron orbital of Cd atom, leading to a decrease in the electron cloud density of the ligands and a higher binding energy peak occurred (Yang et al., 2020). These findings indicate that functional groups (i.e., -NH_2, -COOH, -OH, C-O, and C-N) are responsible for Cd(II) adsorption over BSCs-MEPs.

An indirect impaction by MEPs on the sorption process of Cd(II) onto BSC, as assumed previously, was verified using P 2p high-resolution spectrum. Results shown in Fig. S7 indicate no explicit distinction after adsorption for P compounds. However, MEPs remarkable change the -NH_2 groups on BSCs. There were mainly -NH_3^+ and rare -NH_2 groups (data show none) on BSCs or MEPs (Fig. S6), while the combination of MEPs led to the emergence of -NH_2 on BSCs (Fig. 6c). That is, the affinity of Cd(II) to the BSCs surface, resulting from the used of MEPs, was enhanced by prompting -NH_3 de-protonation, which decreased the positive surface charge and increased the active sites, ultimately resulting in the promotion of Cd(II) adsorption. The following reactions may involve the role of the N, O-containing groups in Cd(II) adsorption (Yan et al., 2018):

$$-CN + Cd^{2+} \rightarrow -CNCd$$
$$-CO + Cd^{2+} \rightarrow -COCd$$
$$-O^{-} + Cd^{2+} \rightarrow -OCd$$
$$-COO^{-} + Cd^{2+} \rightarrow -COOCd$$
$$-NH_3^{+} \rightarrow -NH_2 + H^{+}$$
$$-NH_2 + Cd^{2+} \rightarrow -NH_2Cd$$
$$-OH + -NH_2Cd \rightarrow -NH_2CdOH-$$

Expanding the number of active sites on BSCs available for Cd(II) sorption is an obvious approach to augmenting the adsorption capacity, but the thing is, these active sites are also appropriate for Ca^{2+} (Wei et al., 2021). The mechanism of selective adsorption of Cd is still challenging to determine using traditional chemical methods, while molecular dynamics simulation offer a practical approach to understanding the underlying rule of the selective adsorption process (Fu & Huang, 2018; Sahu et al., 2018). To distinguish the effect on Cd(II) and Ca(II) adsorption posing by functional groups, three cases of critical functional groups assemblies (-COOH/-OH, -NH_2/-OH, and -PO_4/-OH) were modeled on a single polysaccharides, respectively. After the reaction, the optimized geometries of these three systems and the change in mean-squared displacement (MSD) of the Cd(II) and Ca(II) up to reaction time are shown in Fig. 7, while the diffusion coefficients for both Cd(II) and Ca(II) were calculated in each case (Table 3). The diffusion coefficients (D) of Cd(II) and Ca(II) in the presence of different functional groups decreased in the following orders: (−COOH/−OH) > (−NH_2/−OH) > (−PO_4/−OH), this result was in accordance with the analysis of preceding data that active sites like -NH_2/-COOH were responsible for metal ion adsorption. Notably, the D value of Ca was higher than that of Cd only in the simulation case of the molecule containing -COOH/-OH, while the D value of Cd was much higher than that of Ca when the molecule included -NH_2/-OH (Cd: 0.76×10^{-5} cm^2/s; Ca: 0.39×10^{-5} cm^2/s) and −PO_4/−OH (Cd:

Table 3 Determined diffusion coefficients (D) of Cd(II) and Ca(II) in EPS with different functional groups using MD simulation

Metal ion	*D* ($\times 10^{-5}$ cm^2/s)		
	−COOH/−OH	−NH_2/−OH	−PO_4/−OH
Ca^{2+}	1.28	0.39	0.12
Cd^{2+}	0.99	0.76	0.24

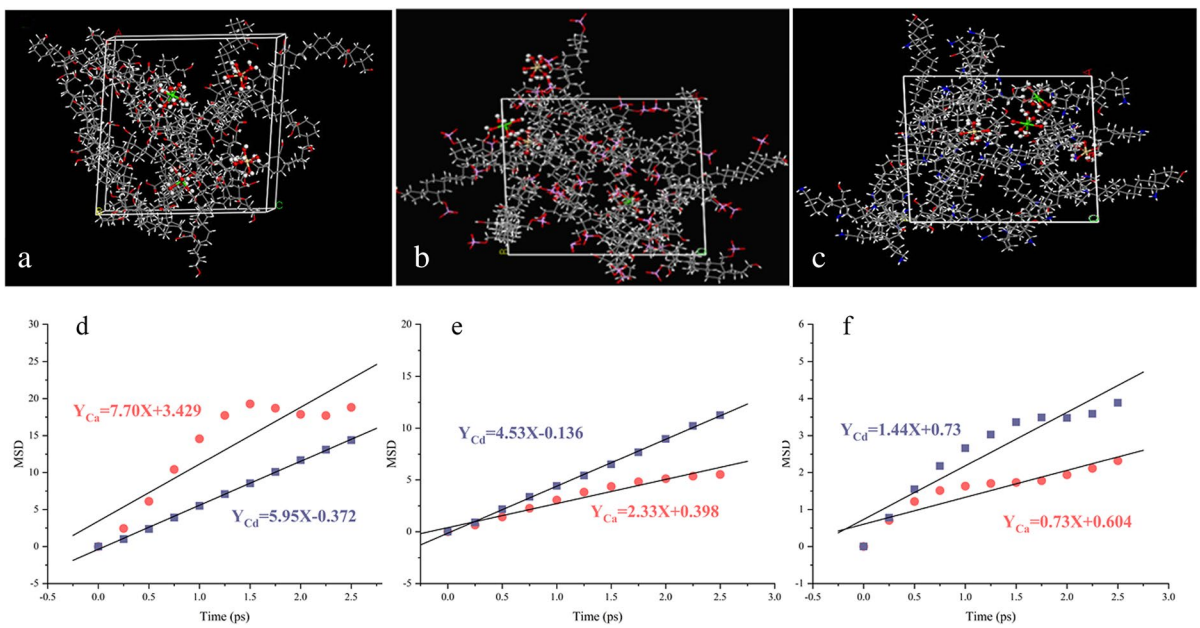

Fig. 7 The optimized geometry (**a**, **b**, **c**) and the mean-squared displacement (MSD) plots (**d**, **e**, **f**) of $Cd^{2+}(H_2O)_4(OH^{-})_2$ and $Ca^{2+}(H_2O)_4(OH^{-})_2$ molecules derived from the MD simulation of those EPs model which individual composed of -COOH/−OH (**a**, **d**), −NH_2/−OH (**b**, **e**), and −PO_4/−OH (**c**, **f**)

0.24×10^{-5} cm^2/s; Ca: 0.12×10^{-5} cm^2/s). This result was equivalent to the slope of the fitted equation and could be considered as the movement rate of ions toward BSCs that illustrated Cd ions were more easily to adsorb on compared to Ca. In addition, the D value of Cd in the system of PO_4-containing molecules was more than twice that of Ca, suggesting that the interaction between PO_4 and Cd may cause MEPs to act as a filter to preferentially adsorbing Cd ions. It has been reported that phosphate could alter the binding sequence of different functional groups and restrict the binding affinity of heavy metals (Ding et al., 2021), which aligns with the results mentioned above.

4 Conclusion

In this study, a synthetic nanomaterial (MEPs) was composited to biological soil crusts (BSCs) and utilized for the removal of Cd(II) from an aqueous solution. It was clearly demonstrated that BSCs-MEPs exhibited better Cd(II) adsorption than BSCs. The kinetics of Cd(II) adsorption by BSCs and BSCs-MEPs were well fitted with a pseudo-second-order model, while the MEPs composited to BSCs can accelerate the rate of adsorption, change the removal process of Cd(II) from 3-stage to 2-stage. The equilibrium adsorption amounts of Cd(II) over BSCs-MEPs have thus been significantly enhanced compared with BSCs. Furthermore, BSCs-MEPs showed improved adsorption capacity over a pH range of 2–9 and exhibited selective adsorption for Cd. Elemental distribution analysis revealed a connection between Cd adsorption and MEPs, while XPS analysis further confirmed that MEPs reduced the positive surface charge, thereby increasing the active sites for Cd adsorption, these changes would be to the benefit of Cd adsorption. Molecular dynamics simulation provides insight into the selection of Cd, in which MEPs act as a filter and Cd thus could be more easily diffused and adsorbed. Generally speaking, our research provides a dependable and credible methodology of Cd removal under an environmental condition of numerous interfering factors. It is important to note that our study, like others, did not observe the selective adsorption process through traditional chemical experiments. Although this process is extremely challenging, future research should prioritize understanding the adsorption behavior of heavy metals on material surfaces at the molecular level, deepen our understanding of this scientific problem by observing and understanding the selective adsorption of molecules through chemical and physical experimental data.

Author Contributions Ke Song: Methodology, Formal analysis, Writing—review & editing. Bin Liu: Experiment operation Investigation. Xiaolin Kuang, Huijuan Song, and Qingru Zeng: Conceptualization, Data curation, Editing. Liang Peng: Funding acquisition, Supervision, Conceptualization, Writing—review & editing.

Funding This work was supported by the National Natural Science Joint Fund (U20A20108) and Key Technologies Research Development Program (2022YFD1700102).

Data Availability Not applicable.

Declarations

Ethics Approval Not applicable.

Consent to Participate Not applicable.

Consent for Publication Not applicable.

Competing Interests The authors declare that they have no competing interests.

References

Abate, G., & Masini, J. C. (2005). Influence of pH, ionic strength and humic acid on adsorption of Cd(II) and Pb(II) onto vermiculite. *Colloids and Surfaces A: Physicochemical and Engineering Aspects, 262*(1–3), 33–39. https://doi.org/10.1016/j.colsurfa.2005.04.005

Büdel, B., & Colesie, C. (2014). *Biological soil crusts* (pp. 131–161). Springer.

Chang, K. S., Chung, Y. C., Yang, T. H., Lue, S. J. J., Tung, K. L., & Lin, Y. F. (2012). Free volume and alcohol transport properties of PDMS membranes: Insights of nanostructure and interfacial affinity from molecular modeling. *Journal of Membrane Science, 417–418*, 119–130. https://doi.org/10.1016/j.memsci.2012.06.019

Cui, L. L., Fan, L., Li, Z. F., Wang, J. J., Chen, R., Zhang, Y. J., Cheng, J. J., Wu, X. L., Li, J. K., Yin, H. Q., Zeng, W. M., & Shen, L. (2021). Characterization of extracellular polymeric substances from Synechocystis sp. PCC6803 under Cd (II), Pb (II) and Cr (VI) stress. *Journal of Environmental Chemical Engineering, 9*(4), 105347. https://doi.org/10.1016/j.jece.2021.105347

Das, S. K., Das, A. R., & Guha, A. K. (2007). A study on the adsorption mechanism of 519 mercury on Aspergillus

versicolor bioweight. *Environmental Science & Technology, 41*(24), 8281–8287. https://doi.org/10.1021/es070814g

Ding, X., Xu, W. H., Li, Z. W., Huang, M., Wen, J. J., Jin, C. S., & Zhou, M. (2021). Phosphate hinders the complexation of dissolved organic matter with copper in lake waters. *Environmental Pollution, 276*, 116739. https://doi.org/10.1016/j.envpol.2021.116739

Elanchezhiyan, S. S., Karthikeyan, P., Rathinam, K., Farzana, M. H., & Park, C. M. (2021). Magnetic kaolinite immobilized chitosan beads for the removal of Pb(II) and Cd(II) ions from an aqueous environment. *Carbohydrate Polymers, 261*(1), 117892. https://doi.org/10.1016/j.carbpol.2021.117892

Fu, W., & Huang, Z. Q. (2018). One-pot synthesis of a two-dimensional porous Fe3O4/Poly(C3N3S3) network nanocomposite for the selective removal of Pb(II) and Hg(II) from synthetic wastewater. *ACS Sustainable Chemistry & Engineering, 6*(11), 14785–14794. https://doi.org/10.1021/acssuschemeng.8b03320

Fulaz, S., Vitale, S., Quinn, L., & Casey, E. (2019). Nanoparticle-biofilm interactions: The role of the EPS matrix. *Trends in Microbiology, 27*(11), 915–926. https://doi.org/10.1016/j.tim.2019.07.004

Gan, C., Liu, Y., Tan, X., Wang, S., Zeng, G., Zheng, B., Li, T., Jiang, Z., & Liu, W. (2015). Effect of porous zinc–biochar nanocomposites on Cr(VI) adsorption from aqueous solution. *RSC Advances, 5*, 35107–35115. https://doi.org/10.1039/c5ra04416b

Gao, J., Xu, G., Qian, H., Liu, P., Zhao, P., & Hu, Y. (2013). Effects of nano-TiO_2 on photosynthetic characteristics of Ulmus elongata seedlings. *Environmental Pollution, 176*, 63–70. https://doi.org/10.1016/j.envpol.2013.01.027

Gillan, D. C. (2016). Metal resistance systems in cultivated bacteria: Are they found in complex communities? *Current Opinion in Biotechnology, 38*, 123–130. https://doi.org/10.1016/j.copbio.2016.01.012

Guo, Z. Z., Zhang, X. D., Kang, Y., & Zhang, J. (2017). Biomass-derived carbon sorbents for Cd(II) removal: Activation and adsorption mechanism. *ACS Sustainable Chemistry & Engineering, 5*(5), 4103–4109. https://doi.org/10.1021/acssuschemeng.7b00061

Hu, S., Lian, F. Q., & Wang, J. F. (2019). Effect of pH to the surface precipitation mechanisms of arsenate and cadmium on TiO2. *Science of the Total Environment, 666*, 956–963. https://doi.org/10.1016/j.scitotenv.2019.02.285

Igiri, B. E., Okoduwa, S. I. R., Idoko, G. O., Akabuogu, E. P., Adeyi, A. Q., & Ejiogu, I. K. (2018). Toxicity and bioremediation of heavy metals contaminated ecosystem from tannery wastewater: A review. *Journal of Toxicology*, 2568038. https://doi.org/10.1155/2018/2568038

Imran, M., Khan, Z. U. K., Iqbal, J., Shah, N. S., Muzammil, S., Ali, S., Muhammad, N., Aziz, A., Murtaza, B., Naeem, M. A., Amjad, M., Shahid, M., Zakir, A., & Rizwan, M. (2020). Potential of siltstone and its composites with biochar and magnetite nanoparticles for the removal of cadmium from contaminated aqueous solutions: Batch and column scale studies. *Environmental Pollution, 259*, 113938. https://doi.org/10.1016/j.envpol.2020.113938

Karthik, R., & Meenakshi, S. (2015). Removal of Pb(II) and Cd(II) ions from aqueous solution using polyaniline grafted chitosan. *Chemical Engineering Journal, 263*, 168–177. https://doi.org/10.1016/j.cej.2014.11.015

Kruglikov, S. S., Nekrasova, N. E., Kuznetsov, V. V., & Filatova, E. A. (2019). An electromembrane process for cadmium recovery from dilute cadmium electroplating dragout solutions. *Membranes and Membrane Technologies, 1*(2), 120–126. https://doi.org/10.1134/S2517751619020057

Kuang, X. L., Shao, J. H., Peng, L., Song, H. J., Wei, X. D., Luo, S., & Gu, J. D. (2020). Nano-TiO2 enhances the adsorption of Cd(II) on biological soil crusts under mildly acidic conditions. *Journal of Contaminant Hydrology, 229*, 103583. https://doi.org/10.1016/j.jconhyd.2019.103583

Kumar, L., Ragunathan, V., Chugh, M., & Bharadvaja, N. (2021). Nanomaterials for remediation of contaminants: A review. *Environmental Chemistry Letters, 19*, 3139–3163. https://doi.org/10.1007/s10311-021-01212-z

Kumar, V., Parihar, R. D., Sharma, A., Bakshi, P., Sidhu, G. P. S., Bali, A. S., Karaouzas, I., Bhardwaj, B., Thukral, A. K., Gyasi-Agyei, Y., & Rodrigo-Comino, J. (2019). Global evaluation of heavy metal content in surface water bodies: A meta-analysis using heavy metal pollution indices and multivariate statistical analyses. *Chemosphere, 236*, 124364. https://doi.org/10.1016/j.chemosphere.2019.124364

Li, B., Peng, L., Wei, D. N., Lei, M., Liu, B., Lin, Y. Q., Li, Z. Y., & Gu, J. D. (2017). Enhanced flocculation and sedimentation of trace cadmium from irrigation water using phosphoric fertilizer. *Science of the Total Environment, 485*, 601–602. https://doi.org/10.1016/j.scitotenv.2017.05.160

Li, G. Y., Yan, L. J., Chen, X. M., Lam, S. S., Rinklebe, J., Yu, Q., Yang, Y. F., Peng, W. X., & Sonne, C. (2023). Phytoremediation of cadmium from soil, air and water. *Chemosphere, 320*, 138058. https://doi.org/10.1016/j.chemosphere.2023.138058

Lian, Z. Y., Yang, Z. Y., Song, W. F., Sun, M. G., Gan, Y., & Bai, X. Y. (2022). Effects of different exogenous cadmium compounds on the chemical composition and adsorption properties of two gram-negative bacterial EPS. *Science of the Total Environment, 806*(Part 1), 150511. https://doi.org/10.1016/j.scitotenv.2021.150511

Liu, L., Yue, T., Liu, R., Lin, H., Wang, D. Q., & Li, B. X. (2021a). Efficient absorptive removal of Cd(II) in aqueous solution by biochar derived from sewage sludge and calcium sulfate. *Bioresource Technology, 336*, 125333. https://doi.org/10.1016/j.biortech.2021.125333

Liu, L., Zhao, J., Liu, X., Bai, S., Lin, H., & Wang, D. (2021b). Reduction and removal of As(V) in aqueous solution by biochar derived from nano zero-valent-iron (nZVI) and sewage sludge. *Chemosphere, 277*, 130273. https://doi.org/10.1016/j.chemosphere.2021.130273

Liu, T., Chen, Z. S., Li, Z. X., Chen, G. L., Zhou, J. L., Chen, Y. Q., Zhu, J. W., & Chen, Z. (2021c). Rapid separation and efficient removal of Cd based on enhancing surface precipitation by carbonate-modified biochar. *ACS Omega, 6*, 18253–18259. https://doi.org/10.1021/acsomega.1c02126

Lu, H., Zhang, W., Yang, Y., Huang, X. F., Wang, S. Z., & Qiu, R. L. (2012). Relative distribution of Pb^{2+} sorption

mechanisms by sludge-derived biochar. *Water Research, 46*(3), 854–862. https://doi.org/10.1021/acsomega.1c02126

Mansoorianfar, M., Nabipour, H., Pahlevani, F., Zhao, Y. W., Hussain, Z., Hojjati-Najafabadi, A., Hoang, H. Y., & Pei, R. J. (2022). Recent progress on adsorption of cadmium ions from water systems using metal-organic frameworks (MOFs) as an efficient class of porous materials. *Environmental Research, 214*(Part 4), 114113. https://doi.org/10.1016/j.envres.2022.114113

Martinez, R. E., Smith, D. S., Kulczycki, E., & Ferris, F. G. (2002). Determination of intrinsic bacterial surface acidity constants using a donnan shell model and a continuous pK(a) distribution method. *Journal of Colloid and Interface Science, 253*, 130e139. https://doi.org/10.1006/jcis.2002.8541

Mathivanan, K., Chandirika, J. U., Mathimani, T., Rajaram, R., Annadurai, G., & Yin, H. Q. (2021). Production and functionality of exopolysaccharides in bacteria exposed to a toxic metal environment. *Ecotoxicology and Environmental Safety, 208*, 111567. https://doi.org/10.1016/j.ecoenv.2020.111567

Metwally, S. S., & Rizk, H. E. (2014). Preparation and characterization of nano-sized iron-titanium mixed oxide for removal of some lanthanides from aqueous solution. *Separation Science and Technology, 49*(15), 2426–2436. https://doi.org/10.1080/01496395.2014.926457

Nabipour, H., Rohani, S., Batool, S., & Yusuff, A. S. (2023). An overview of the use of water-stable metal-organic frameworks in the removal of cadmium ion. *Journal of Environmental Chemical Engineering, 11*(1), 109131. https://doi.org/10.1016/j.jece.2022.109131

Nouha, K., Kumar, R. S., & Tyagi, R. D. (2016). Heavy metals removal from wastewater using extracellular polymeric substances produced by Cloacibacterium normanense in wastewater sludge supplemented with crude glycerol and study of extracellular polymeric substances extraction by different methods. *Bioresource Technology, 212*, 120–129. https://doi.org/10.1016/j.biortech.2016.04.021

Peng, L., Zhou, S. Y., Song, H. J., Yang, Y. H., Lei, M., & Zhou, F. (2020). Enhanced Selective Removal of Cd(II)by an Amino-Functional Water-Retaining Agent Incorporating Nano Hydrous Manganese Oxide. *Journal ofNanoscience and Nanotechnology, 20*(9), 5906–5915. https://doi.org/10.1166/jnn.2020.18546

Peng, Z. D., Lin, X. M., Zhang, Y. L., Hu, Z., Yang, X. J., Chen, C. Y., Chen, H. Y., Li, Y. T., & Wang, J. J. (2021). Removal of cadmium from wastewater by magnetic zeolite synthesized from natural, low-grade molybdenum. *Science of the Total Environment, 772*, 145355. https://doi.org/10.1016/j.scitotenv.2021.145355

Qu, C. C., Yang, S. S., Mortimer, M., Zhang, M., Chen, J. Z., Wu, Y. C., Chen, W. L., Cai, P., & Huang, Q. Y. (2022). Functional group diversity for the adsorption of lead(Pb) to bacterial cells and extracellular polymeric substances. *Environmental Pollution, 295*, 118651. https://doi.org/10.1016/j.envpol.2021.118651

Rao, G. R., Meher, S. K., Mishra, B. G., & Charan, P. H. K. (2012). Nature and catalytic activity of bimetallic CuNi particles on CeO_2 support. *Catalysis Today, 198*(1), 140–147. https://doi.org/10.1016/j.cattod.2012.06.027

Saleh, T. A., Mustaqeem, M., & Khaled, M. (2022). Water treatment technologies in removing heavy metal ions from wastewater: A review. *Environmental Nanotechnology, Monitoring & Management, 17*, 100617. https://doi.org/10.1016/j.enmm.2021.100617

Sahu, P., Singha Deb, A. K., Ali, S. K. M., Shenoy, K. T., & Mohan, S. (2018). Tailoring of carbon nanotubes for the adsorption of heavy metal ions. *Molecular Dynamics and Experimental Investigations, 3*(6), 917–929.https://doi.org/10.1039/C8ME00039E

Shashkova, I. L., Rat'ko, A. I., & Kitikova, N. V. (1999). Removal of heavy metal ions from aqueous solutions by alkaline-earth metal phosphates. *Colloids and Surfaces A: Physicochemical and Engineering Aspects, 160*(3), 207–215. https://doi.org/10.1016/S0927-7757(99)00193-4

Shirkhorshidi, B., Ghanatghestani, M. D., Moeinpour, F., & Parvaresh, H. (2023a). The impacts of microplastics on sorption and desorption specifications of iron in soil. *Water, Air, & Soil Pollution, 234*, 37. https://doi.org/10.1007/s11270-023-06395-5

Shirkhorshidi, B., Ghanatghestani, M. D., Moeinpour, F., & Parvaresh, H. (2023b). Exploring the interaction between microplastics and heavy metals: Unveiling the impact of microplastics on lead sorption and desorption in soil. *Environmental Monitoring and Assessment, 195*, 1017. https://doi.org/10.1007/s10661-023-11640-9

Song, H. J., Kuang, X. L., Wei, S. D., Luo, S., Zeng, Q. R., & Peng, L. (2022). The effect of TiO_2 nanoparticles size on Cd (II) removal by the paddy crusts from waterbody. *Journal of Environmental Chemical Engineering, 10*(3), 107883. https://doi.org/10.1016/j.jece.2022.107883

Song, L. Z., Zhao, X. D., Fu, J., Wang, X. L., Sheng, Y. P., & Liu, X. W. (2012). DFT investigation of Ni(II) adsorption onto MA-DTPA/PVDF chelating membrane in the presence of coexistent cations and organic acids. *Journal of Hazardous Materials, 199–200*, 433–439. https://doi.org/10.1016/j.jhazmat.2011.11.046

Szczepański, P., Guo, H. P., Dzieszkowski, K., Rafiński, Z., Wolan, A., Fatyeyeva, K., Kujawa, J., & Kujawski, W. (2021). New reactive ionic liquids as carriers in polymer inclusion membranes for transport and separation of Cd(II), Cu(II), Pb(II), and Zn(II) ions from chloride aqueous solutions. *Journal of Membrane Science, 638*, 119674. https://doi.org/10.1016/j.memsci.2021.119674

Tang, K., Yuan, B., Jia, L., Pan, X., Feng, F., & Jin, K. (2021). Spatial and temporal distribution of aerobic anoxygenic phototrophic bacteria: Key functional groups in biological soil crusts. *Environmental Microbiology, 23*, 3554–3567. https://doi.org/10.1111/1462-2920.15459

Tang, S., Yang, K., Liu, F., Peng, M., Yang, Z., Liu, X. J., Guo, F., & Ma, H. H. (2022). Overview of heavy metal pollution and health risk assessment of urban soils in Yangtze River Economic Belt, China. *Environmental Geochemistry and Health, 44*, 4455–4497. https://doi.org/10.1007/s10653-022-01210-2

Teng, D., Zhang, B., Xu, G., Wang, B., Mao, K., Wang, J., Sun, J., Feng, X., Yang, Z., & Zhang, H. (2020). Efficient removal of Cd(II) from aqueous solution by pinecone biochar: Sorption performance and governing mechanisms.

Environmental Pollution, 265, 115001. https://doi.org/10.1016/j.envpol.2020.115001

Tiwari, O. N., Bhunia, B., Mondal, A., Gopikrishna, K., & Indrama, T. (2019). System metabolic engineering of exopolysaccharide-producing cyanobacteria in soil rehabilitation by inducing the formation of biological soil crusts: A review. *Journal of Cleaner Production, 211*, 70–82. https://doi.org/10.1016/j.jclepro.2018.11.188

Tran, T. K., Kim, N., Le, Q. C., Nguyen, M. T., Leu, H. J., & Vo Thi, K. N. (2021). Electrochemical preparation and characterization of polyaniline enhanced electrodes: An application for the removal of cadmium metals in industrial wastewater. *Materials Chemistry and Physics, 261*, 124221. https://doi.org/10.1016/j.matchemphys.2021.124221

Vassilev, S. V., Vassileva, C. G., & Bai, J. (2023). Content, modes of occurrence, and significance of phosphorous in biomass and biomass ash. *Journal of the Energy Institute, 108*, 101205. https://doi.org/10.1016/j.joei.2023.101205

Wang, L. L., Shi, Y., Yao, D. K., Pan, H., Hou, H. J., Chen, J., & Crittenden, J. C. (2019). Cd complexation with mercapto-functionalized attapulgite (MATP): Adsorption and DFT study. *Chemical Engineering Journal, 366*, 569–576. https://doi.org/10.1016/j.cej.2019.02.114

Warren, S. D., Rosentreter, R., & Pietrasiak, N. (2021). Biological soil crusts of the great plains: A review. *Rangeland Ecology & Management, 78*, 213–219. https://doi.org/10.1016/j.rama.2020.08.010

Wei, X. F., Chen, S. C., Rong, J. J., Sui, Z. X., Wang, S. J., Lin, Y. B., Xiao, J. H., & Huang, D. W. (2021). Improving the Ca(II) adsorption of chitosan via physical and chemical modifications and charactering the structures of the calcified complexes. *Polymer Testing, 98*, 107192. https://doi.org/10.1016/j.polymertesting.2021.107192

Wu, M., Liu, B., Li, J., Su, X. T., Liu, W. Z., & Li, X. Q. (2023). Influence of pyrolysis temperature on sludge biochar: The ecological risk assessment of heavy metals and the adsorption of Cd(II). *Environmental Science and Pollution Research, 30*, 12608–12617. https://doi.org/10.1007/s11356-022-22827-x

Wyatt, M. A., Johnston, C. W., & Magarvey, N. A. (2014). Gold nanoparticle formation via microbial metallophore chemistries. *Journal of Nanoparticle Research, 16*, 2212. https://doi.org/10.1007/s11051-013-2212-2

Yan, S. J., Cai, Y. G., Li, H. Q., Song, S. X., & Xia, L. (2022). Enhancement of cadmium adsorption by EPS-montmorillonite composites. *Environmental Pollution, 252*(Part B), 1509–1518. https://doi.org/10.1016/j.envpol.2019.06.071

Yan, Z., Fu, L., & Yang, H. (2018). Functionalized 2D clay derivative: hybrid nanosheets with unique lead sorption behaviors and interface structure. *Advanced Materials Interfaces, 5*, 1700934. https://doi.org/10.1002/admi.201700934

Yang, J., Liu, J. Z., Wu, C. X., Kerr, P. G., Wong, P., & Wu, Y. H. (2016). Bioremediation of agricultural solid waste leachates with diverse species of Cu (II) and Cd (II) by periphyton. *Bioresource Technology, 221*, 214–221. https://doi.org/10.1016/j.biortech.2016.09.048

Yang, J., Tang, C. L., Wang, F. W., & Wu, Y. H. (2015a). Co-contamination of Cu and Cd in paddy fields: Using periphyton to entrap heavy metals. *Journal of Hazardous Materials, 304*, 150–158. https://doi.org/10.1016/j.jhazmat.2015.10.051

Yang, J., Wei, W., Pi, S. S., Ma, F., Li, A., Wu, D., & Xing, J. (2015b). Competitive adsorption of heavy metals by extracellular polymeric substances extracted from Klebsiella sp. J1. *Bioresource Technology, 196*, 533–539. https://doi.org/10.1016/j.biortech.2015.08.011

Yang, Z. H., Chen, X. H., Li, S. Y., Ma, W. H., Li, Y., He, Z. D., Hu, H. R., & Wang, T. (2020). Effective removal of Cd(II) from aqueous solution based on multifunctional nanoporous silicon derived from solar kerf loss waste. *Journal of Hazardous Materials, 385*, 121522. https://doi.org/10.1016/j.jhazmat.2019.121522

Yenial, Ü., & Bulut, G. (2017). Examination of flotation behavior of metal ions for process water remediation. *Journal of Molecular Liquids, 241*, 130–135. https://doi.org/10.1016/j.molliq.2017.06.011

Yue, Z. B., Li, Q., Li, C. C., Chen, T. H., & Wang, J. (2015). Component analysis and heavy metal adsorption ability of extracellular polymeric substances (EPS) from sulfate reducing bacteria. *Bioresource Technology, 194*, 399–402. https://doi.org/10.1016/j.biortech.2015.07.042

Zawierucha, I., & Nowik-Zajac, A. (2019). Evaluation of permeable sorption barriers for removal of Cd(II) and Zn(II) ions from contaminated groundwater. *Water Science and Technology, 80*(3), 448–457. https://doi.org/10.1016/j.biortech.2015.07.042

Zhang, Z., Wang, T., Zhang, H., Liu, Y., & Xing, B. S. (2021). Adsorption of Pb(II) and Cd(II) by magnetic activated carbon and its mechanism. *Science of the Total Environment, 757*, 143910. https://doi.org/10.1016/j.scitotenv.2020.143910